Topological Defects and Misfit Strain in Magnetic Stripe Domains of Lateral Multilayers With Perpendicular Magnetic Anisotropy

A. Hierro-Rodriguez,[1,2] R. Cid,[1,2] M. Vélez,[1,*] G. Rodriguez-Rodriguez,[1,2] J. I. Martín,[1,2] L. M. Álvarez-Prado,[1,2] and J. M. Alameda[1,2]

[1]*Departamento de Física, Universidad de Oviedo, 33007 Oviedo, Spain*
[2]*CINN, (CSIC-UO-P. Asturias), Llanera, Spain*

(Received 26 April 2012; published 11 September 2012)

Stripe domains are studied in perpendicular magnetic anisotropy films nanostructured with a periodic thickness modulation that induces the lateral modulation of both stripe periods and in-plane magnetization. The resulting system is the 2D equivalent of a strained superlattice with properties controlled by interfacial misfit strain within the magnetic stripe structure and shape anisotropy. This allows us to observe, experimentally for the first time, the continuous structural transformation of a grain boundary in this 2D magnetic crystal in the whole angular range. The magnetization reversal process can be tailored through the effect of misfit strain due to the coupling between disclinations in the magnetic stripe pattern and domain walls in the in-plane magnetization configuration.

DOI: 10.1103/PhysRevLett.109.117202 PACS numbers: 75.60.Jk, 75.70.Kw, 75.75.−c

Stripe domains in ferromagnetic films with perpendicular magnetic anisotropy (PMA) present a fascinating variety of configurations ranging from ordered parallel states to disordered labyrinthine patterns that depend both on material parameters and magnetic and thermal history [1,2]. They share a common phenomenology with many other systems with self-organized patterns such as microdomains in block copolymer thin films [3], wrinkles in elastic membranes [4], or liquid crystals [5]. The physics of stripe domains is a basic issue both to understand magnetic hysteresis loops in PMA materials [6,7] for technology applications and to unravel the different phase transitions that appear in 2D [8,9]. Studies performed in extended systems have revealed the complex phase diagram of these modulated phases [1,9,10] and the important role of topological defects in order-disorder mechanisms [3,11]. The actual pattern realized in a given extended sample depends on the interplay between the equilibrium periodic configuration and the strain present in the magnetic system and is controlled by the motion of topological defects such as dislocations, disclinations, and grain boundaries [12,13]. On the other hand, magnetic stripes in nanostructured systems, such as dots, rings, and wires of PMA materials [14–16] or copolymers nucleated in periodic gratings [17] show much simpler patterns due to the coupling between shape and domain structure [10].

Recently, the concept of magnetic lateral multilayer, i.e., an extended film with a laterally nanostructured magnetic property such as anisotropy [18], saturation magnetization [19], or exchange bias [20], has emerged as a bridge between extended and confined geometries. These laterally nanostructured samples combine confinement effects and coupling effects between nearby elements similar to those found in the more standard geometry of vertical multilayers. In this framework, magnetic stripe domains in an extended PMA film can be considered as a bulk 2D crystal of lattice parameter λ. Then, a lateral periodic modulation of λ would result in the 2D equivalent of 3D strained superlattices fabricated by the alternate deposition of layers with different lattice constants [21,22]. Thus, in the same way as homogeneous and random strains on the magnetic stripe pattern of extended samples have a significant influence in their effective magnetization configuration, the presence of localized strain at the interfaces of a lateral magnetic stripe multilayer can provide an extra control over the magnetic hysteresis loop.

In this Letter, we study the magnetic stripe domain structure in lateral multilayers fabricated on nanostructured PMA films with periodic thickness modulation. This has allowed us to observe experimentally, for the first time, the continuous transformation of a grain boundary in this 2D magnetic crystal in the whole angular range driven by misfit strain and, also, how the coupling between topological defects in the magnetic stripe structure and the underlying in-plane magnetization configuration can be used to tailor the magnetization reversal process.

Amorphous 80 nm $NdCo_5$ alloy films have been grown by sputtering on 10 nm Al/Si(100) substrates, and protected from oxidation with a 3 nm Al capping layer [23]. At room temperature, the saturation magnetization is $M_S = 1100$ emu/cm^3 and the PMA K_N is of the order of 10^6 erg/cm^3 [23,24]. They have been characterized by transverse magneto-optical Kerr effect with the field H applied parallel to the sample plane and by magnetic force microscopy (MFM) using a Nanotec^{TM} system with a 1 kOe electromagnet to apply an in-plane variable H [25]. Figure 1(a) is a MFM image taken at remanence after applying $H = 1$ kOe that displays a well defined stripe domain structure, aligned along the direction of the last saturating field. The fast Fourier transform (FFT) of this

image [top inset of Fig. 1(a)] displays two symmetric peaks that provide precise information about the angular orientation of the stripe pattern and its periodicity ($\lambda = 157$ nm). The in-plane hysteresis loop [bottom inset of Fig. 1(a)] is a typical *transcritical* loop with a linear reversible region at high fields, characteristic of PMA materials. The finite value of the remanent magnetization $0.4M_S$ indicates that, besides the oscillating out-of-plane magnetization component that gives rise to the black-white MFM contrast, there is a significant average in-plane magnetization component M_{parallel}, lying along the stripe domain direction [10,24,26,27].

For a given set of parameters (M_S, K_N, H), both λ and M_{parallel} are a function of sample thickness t [7,28,29]. Thus, a nanostructured sample composed of alternate linear regions of thickness t_1 and t_2, as sketched in Fig. 1(b), would also present a similar lateral modulation in λ and M_{parallel} that is the aim of our work. In the following, we will refer to the stripe period and in-plane magnetization component in the thin and thick regions as λ_1, M_1 and λ_2, M_2, respectively. A two step lithography process has been performed for sample fabrication. First, 70×70 μm^2 flat squares of 80 nm thick Nd-Co film have been defined by a combined e-beam lithography and lift-off process. Then, a mask of equispaced parallel 70 μm long 10 nm thick Nb lines is defined on top of the squares by a second combined e-beam lithography and lift-off process. This pattern of lines is transferred to the underlying Nd-Co film by ion beam etching with Ar^+ ions, creating a set of linear grooves of depth Δt controlled by etching time. Finally, the sample is covered by a 3 nm Al capping layer. The result is a film with alternate linear regions of thickness $t_1 = 80$ nm $- \Delta t$ and $t_2 = 80$ nm, width $w/2$ and lateral period w. Two series of samples have been fabricated either with shallow ($\Delta t = 12$ nm) or deep ($\Delta t = 30$ nm) grooves and $w = 0.5$, 1, 1.4, and 2 μm, in order to analyze the behavior of these lateral multilayers in the two limits of either small or large amplitude thickness modulation. A flat 70 μm Nd-Co square has also been defined near each nanostructured sample for control purposes.

Figure 2(a) shows the MFM image of a Nd-Co sample with shallow grooves ($\Delta t = 12$ nm) and $w = 2$ μm taken in $H = 1$ kOe applied at $\theta \simeq 90°$, showing a well defined magnetic stripe pattern oriented along H. The effect of nanostructuring in their configuration is clear: the thinner regions, present weaker and more closely spaced stripes with $\lambda_1 = 132$ nm, whereas in the thicker regions the stripes show a stronger contrast and a larger period $\lambda_2 = 144$ nm (topography images have been used as a mask to select the relevant area for the FFT analysis of stripe periods in thin and thick regions).

Several dislocations can be identified within the magnetic stripe pattern, about half of them located at the edges between thin-thick lines: two dislocations appear in the left-most edge, whereas four dislocations can be counted in the central edge. In all the cases, they correspond to the addition of an extra stripe to the pattern in the thin region; i.e., they can be identified as misfit dislocations. In the control 80 nm flat film, measured at the same conditions, the magnetic stripe period is $\lambda_0 = 151$ nm and only 3 dislocations can be seen in a similar 3×3 μm^2 area. Thus, two kinds of strains appear in the magnetic system: first, an effective misfit strain that can be defined as

$$\delta_{\text{misfit}} = \frac{\lambda_1 - \lambda_2}{\lambda_2}, \tag{1}$$

and is relaxed by misfit dislocations; second, a residual strain due to the difference with the equilibrium magnetic stripe period that results in elastic energy stored in the system. In this case, $\delta_{\text{misfit}} = -0.083$ which, taking the Burgers vector $b = 132$ nm, implies an average misfit dislocation spacing [21,22] $D = b/|\delta_{\text{misfit}}| = 1580$ nm. This is equivalent to two dislocations in a 3 μm long edge, which is qualitatively in agreement with the observed numbers in Fig. 2(a).

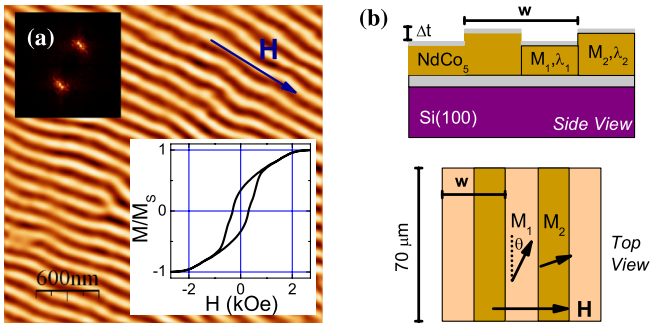

FIG. 1 (color online). (a) MFM image of stripe domains in a 80 nm thick Nd-Co film at $H = 0$ ($\lambda = 157$ nm). Top inset is the FFT pattern. Bottom inset is the in-plane transverse magneto-optical Kerr effect hysteresis loop. (b) Sketch of the nanostructured Nd-Co samples with periodic thickness modulation. θ is the angle measured relative to the nanostructured lines.

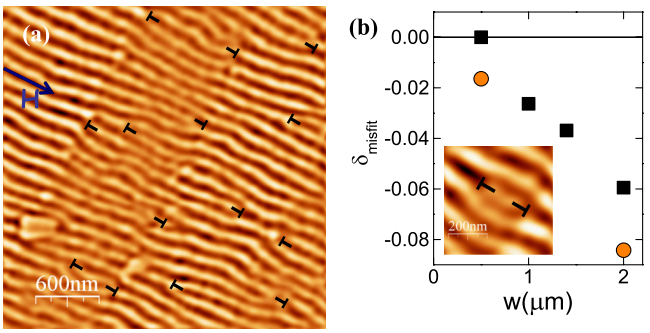

FIG. 2 (color online). (a) 3×3 μm^2 MFM image of stripe domains in nanostructured Nd-Co film ($\Delta t = 12$ nm, $w = 2$ μm) at $H = 1$ kOe. (b) Misfit strain vs lateral periodicity at $H = 1$ kOe: (∘), $\theta \simeq 90°$; (□), $\theta \simeq 5°$. Inset is a detail of misfit dislocations in the sample with $w = 0.5$ μm.

As w decreases, λ values in the thin and thick lines approach to each other and the absolute value of misfit strain becomes smaller both for H parallel and perpendicular to the nanostructured lines [see Fig. 2(b)]. For example, for $w = 0.5\ \mu$m, $\delta_{\text{misfit}} = 0$ with H at $\theta = 5°$ and $\delta_{\text{misfit}} = -0.016$ with H at $\theta = 90°$. In this last case, misfit dislocations appear as closely bound pairs spaced at $w/2$ [see inset of Fig. 2(b)]. This is different from the behavior of isolated PMA wires [16] in which stripe period is independent of wire width for H perpendicular to the edges, remarking the relevance of interaction between magnetic stripes in neighboring lines in our experiment. Actually, the data in Fig. 2(b) follow the characteristic trend of strained superlattices [21,22], in which $|\delta_{\text{misfit}}|$ is an increasing function of layer thickness ($w/2$ in our case) above a critical thickness given by the balance between dislocation and elastic energies. The critical line width here can be estimated as $w_c/2 \approx 250$ nm, which is of the order of $1.5\lambda_0$. That is, for smaller feature sizes misfit strain should be negligible and the magnetic stripe pattern becomes coherent over the whole sample. It can be noted that previous works in patterned PMA films were in this small feature limit (feature size of the order of λ_0) and, thus, only domain pinning effects were reported [30,31].

The magnetization reversal process is almost the same in films with shallow grooves and in flat films: stripe domains stay parallel to H during the whole hysteresis loop with a small enhancement in λ at the coercivity, in a similar way as reported for other PMA films [7,29]. However, in the samples with deeper grooves the differences between thin and thick regions are enhanced and the magnetic behavior changes qualitatively. Figure 3 shows a series of MFM images of a nanostructured Nd-Co film ($\Delta t = 30$ nm, $w = 1.4\ \mu$m) taken at increasing fields after saturation at $H = -1$ kOe perpendicular to the lines [24]. In the thin regions, a well defined pattern of parallel stripes is seen in all the images that rotates in a continuous fashion away from the applied field direction and becomes aligned to the nanostructured lines at coercivity ($H_C = 90$ Oe). On the other hand, stripes in the thick regions remain always oriented approximately along the applied field direction but develop a labyrinthine structure at coercivity. Thus, a variable angle grain boundary appears at the interface between thin and thick lines that undergoes a continuous structural transformation during the magnetization reversal process.

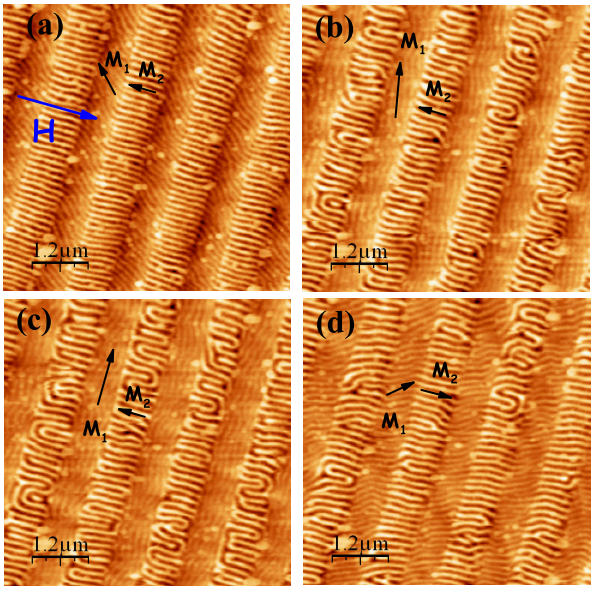

FIG. 3 (color online). $6 \times 6\ \mu$m^2 MFM images of stripe domains in nanostructured Nd-Co film ($\Delta t = 30$ nm, $w = 1.4\ \mu$m) taken after saturation at $H = -1$ kOe at: (a) $H = -12$ Oe; (b) $H = 74$ Oe; (c) $H = 96$ Oe; (d) $H = 150$ Oe. Arrows indicate the positive sense of the applied field and the average in-plane magnetization in the thick and thin regions.

The magnetization rotation in the thin regions [see Fig. 4(a)] can be attributed to the effective shape anisotropy created by the flux discontinuities that appear at the interface between thin and thick lines due to the lateral modulation of the in-plane magnetization [32]. In this framework, the leading energy terms within the thin lines correspond to the dipolar and Zeeman terms. Then, the energy density e for M_1 oriented at θ relative to the lines, M_2 at 90° and H at θ_0 may be written as:

$$e = 2\pi N_x (M_1 \sin\theta - M_2)^2 - HM_1 \cos(\theta - \theta_0), \quad (2)$$

with N_x the demagnetizing factor perpendicular to the lines. Thus, the equilibrium magnetization orientation would be given by

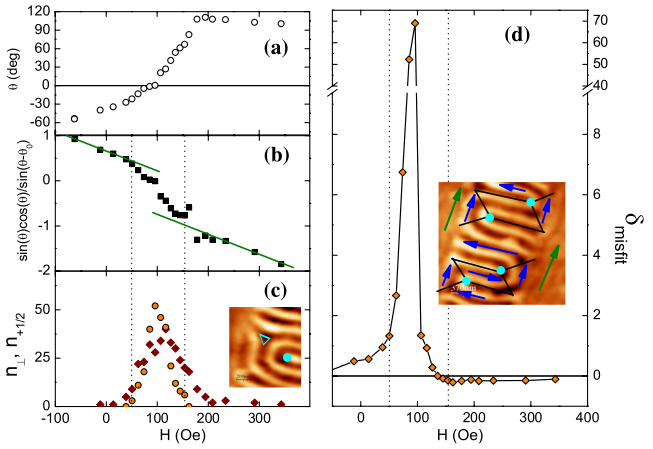

FIG. 4 (color online). (a) Field dependence of the orientation angle of M_1 relative to the lines. (b) Equilibrium condition for coherent rotation in the thin regions with $\theta_0 = 95°$. Solid lines are linear fits to Eq. (3). (c) Number of dislocations $n_\perp$ (◇) and $+1/2$ disclinations $n_{+1/2}$ (∘) in the thick regions vs H. Dotted lines indicate the H range of disclination observation. Inset is a detail of a disclination dipole of Burgers vector $3\lambda_2$. (d) δ_{misfit} vs H. Inset is a sketch of the in-plane magnetization configuration for a buckled stripe pattern. ∘ and △ indicate $+1/2$ and $-1/2$ disclinations, respectively.

$$H = -4\pi N_x M_1 \frac{\sin\theta\cos\theta}{\sin(\theta-\theta_0)} + 4\pi N_x M_2 \frac{\cos\theta}{\sin(\theta-\theta_0)}. \quad (3)$$

The first term corresponds to a rotation process under an anisotropy field $H_K = 4\pi N_x M_1$ and the second to the bias field created by the thick lines $H_D = 4\pi N_x M_2$ weighed by an angular factor that is close to unity for $\theta_0 \approx 90°$. Figure 4(b) is a plot of $\sin\theta\cos\theta/\sin(\theta-\theta_0)$ vs H with $\theta_0 = 95°$. A linear behavior appears both for $H < 50$ and $H > 150$ Oe with $H_K = 235$ Oe in both cases and $H_D = -135$ and 70 Oe respectively. Since H_D and M_2 are proportional, the change of sign in H_D can be taken as a signature of magnetization reversal in the thick regions.

Actually, it is in the intermediate range 50 Oe $< H <$ 150 Oe where the most important structural transformations occur in the magnetic stripe pattern of the thick lines: disclination dipoles appear in the magnetic system and misfit strain reaches its maximum [see Figs. 4(c) and 4(d)]. These changes are a direct consequence of the rotation of M_1 away from the field direction. The stripe spacing projected along the interface between thick and thin regions is $\lambda_1^{\parallel} = \lambda_1/\sin\theta$. Therefore, $\delta_{\text{misfit}} = (\lambda_1^{\parallel} - \lambda_2)/\lambda_2$ is gradually enhanced from $\delta_{\text{misfit}} = 0.5$ to 1.3 as θ goes from $-40°$ at remanence to $-23°$ at 50 Oe. At the same time, a very large density of misfit dislocations is observed in the MFM images. Eventually, at $\delta_{\text{misfit}} \approx 1$, the distance between simple dislocations of Burgers vector $b = \lambda_2$ reaches its minimum value $D = \lambda_2$. Thus, in order to accommodate the increasing strain, dislocations with larger $b = 2\lambda_2, 3\lambda_2, \ldots$ should be nucleated. Instead, the MFM images reveal the existence of a large number $n_{+1/2}$ of $+1/2$ disclinations within the thick regions in this intermediate field range [see Fig. 4(c)].

In 2D, a dislocation is equivalent to a closely bound pair of $+1/2$ and $-1/2$ disclinations that can decay into a disclination dipole either by the effect of temperature or strain [1,3]. One such disclination dipole of Burgers vector $3\lambda_2$ is shown in the inset of Fig. 4(c). As δ_{misfit} is dilative in the thick regions and compressive in the thin ones, $+1/2$ disclinations are mostly observed in the first case whereas $-1/2$ disclinations stay at the other side of the interface. $n_{+1/2}$ reaches its maximum at the coercivity, corresponding to the maximum misfit strain in the magnetic system. Then, $n_{+1/2}$ decreases gradually with a certain lag relative to the relaxation of δ_{misfit}, until all the disclination dipoles are recombined into dislocations for H above 150 Oe.

These $+1/2$ singularities in the stripe pattern are directly coupled to the in-plane magnetization by the Bloch character of the domain walls in between black-white stripes [24]. In this framework, $+1/2$ disclinations are equivalent to 180° domain walls in M_2 together with a half vortex closure structure, as sketched in the inset of Fig. 4(d). In fact, domain walls in nanowires with in-plane magnetization have already been described in terms of pairs of $1/2$ topological defects located at the nanowire edges [33]. The loss of orientational order within the magnetic stripe pattern associated to the presence of disclination dipoles is equivalent to the nucleation of a multidomain structure during magnetization reversal. This is seen from the comparison of Figs. 4(b) and 4(c): the field range where $+1/2$ disclinations are observed corresponds to the transition from negative to positive H_D in the fits to Eq. (3) (i.e., negative to positive M_2). Also, it is interesting to consider that, as in this field range θ approaches zero (i.e., M_2 becomes perpendicular to M_1), the in-plane closure domain structure associated to the disclination dipoles helps to minimize the density of magnetic poles at the interfaces. Thus, the magnetization reversal in this sample with deep nanostructured grooves is a combination of two mechanisms: magnetization rotation of M_1 due to the line shape anisotropy and an incoherent process that reverses M_2 by the nucleation of 180° walls linked to $+1/2$ disclinations within the magnetic stripe pattern above a critical misfit strain $\delta_{\text{misfit}} = 1$.

In summary, a lateral modulation of magnetic stripe periods has been achieved by introducing a periodic thickness modulation in PMA Nd-Co films. In the resulting lateral strained superlattice, magnetic stripe patterns are controlled by the interplay between interfacial misfit strain and shape anisotropy induced by nanostructuring. For deep nanostructured grooves, high angle boundaries appear in the 2D magnetic stripe pattern during in-plane magnetization reversal. The structural changes in these boundaries, driven by misfit strain, determine the magnetic behavior of the system: the decay of high Burgers vector dislocations into disclination dipoles above a critical misfit strain can be directly linked to the nucleation of reversed magnetic domains within the thicker regions.

Work supported by Spanish MICINN under Grant No. FIS2008-06249.

*mvelez@uniovi.es

[1] M. Seul and D. Andelman, Science **267**, 476 (1995).
[2] M. Seul and R. Wolfe, Phys. Rev. A **46**, 7519 (1992)
[3] C. Harrison, D. H. Adamson, Z. Cheng, J. M. Sebastian, S. Sethuraman, D. A. Huse, R. A. Register, and P. M. Chaikin, Science **290**, 1558 (2000).
[4] P. Kim, M. Abkarian, and H. A. Stone, Nature Mater. **10**, 952 (2011).
[5] J. Maclennan and M. Seul, Phys. Rev. Lett. **69**, 2082 (1992).
[6] A. Berger, S. Mangin, J. McCord, O. Hellwig, and E. E. Fullerton, Phys. Rev. B **82**, 104423 (2010).
[7] E. Sallica Leva, R. C. Valente, F. Martinez Tabares, M. Vasquez Mansilla, S. Roshdestwensky, and A. Butera, Phys. Rev. B **82**, 144410 (2010).
[8] D. R. Nelson and B. I. Halperin, Phys. Rev. B **19**, 2457 (1979).

[9] N. Saratz, A. Lichtenberger, O. Portmann, U. Ramsperger, A. Vindigni, and D. Pescia, Phys. Rev. Lett. **104**, 077203 (2010).
[10] D. Clarke, O. A. Tretiakov, and O. Tchernyshyov, Phys. Rev. B **75**, 174433 (2007).
[11] N. Abu-Libdeh and D. Venus, Phys. Rev. B **84**, 094428 (2011).
[12] E. Asciutto, C. Roland, and C. Sagui, Phys. Rev. E **72**, 021504 (2005).
[13] Z. F. Huang and J. Viñals, Phys. Rev. E **75**, 056202 (2007).
[14] M. Hehn, K. Ounadjela, J. P. Bucher, F. Rousseaux, D. Decanini, B. Bartenlian, and C. Chappert, Science **272**, 1782 (1996).
[15] D. Navas, C. Nam, D. Velazquez, and C. A. Ross, Phys. Rev. B **81**, 224439 (2010).
[16] S. H. Lee, F. Q. Zhu, C. L. Chien, and N. Markovic, Phys. Rev. B **77**, 132408 (2008)
[17] D. Sundrani and S. J. Sibener, Macromolecules **35**, 8531 (2002).
[18] S. P. Li, W. S. Lew, J. A. C. Bland, L. Lopez-Diaz, C. A. F. Vaz, M. Natali, and Y. Chen, Phys. Rev. Lett. **88**, 087202 (2002).
[19] J. McCord, L. Schultz, and J. Fassbender, Adv. Mater. **20**, 2090 (2008).
[20] K. Theis-Bröhl, M. Wolff, A. Westphalen, H. Zabel, J. McCord, V. Höink, J. Schmalhorst, G. Reiss, T. Weis, D. Engel, A. Ehresmann, U. Rücker and B. P. Toperverg, Phys. Rev. B **73**, 174408 (2006).
[21] K. Wiesauer and G. Springholz, Phys. Rev. B **69**, 245313 (2004).
[22] Th. Kehagias, Ph. Komninou, G. Nouet, P. Ruterana, and Th. Karakostas, Phys. Rev. B **64**, 195329 (2001).
[23] R. Cid, G. Rodriguez-Rodriguez, L. M. Alvarez-Prado, J. Diaz and J. M. Alameda, J. Magn. Magn. Mater. **316**, e446 (2007).
[24] See Supplemental Material at http://link.aps.org/supplemental/10.1103/PhysRevLett.109.117202 for a brief summary of Nd-Co magnetic properties and weak stripe domain structure and for a movie of the complete hysteresis loop.
[25] F. Valdés-Bango, A. Hierro-Rodriguez, J. M. Teixeira, G. N. Kakazei, Y. G. Pogorelov, G. Rodriguez-Rodriguez, M. Vélez, J. M. Alameda, J. B. Sousa, and J. I. Martin, J. Nanosci. Nanotechnol. **12**, 7510 (2012).
[26] A. Hubert and R. Schäfer, *Magnetic Domains: The Analysis of Magnetic Microstructures* (Springer, Berlin, 1998) p. 298.
[27] L. M. Alvarez-Prado, G. T. Pérez, R. Morales, F. H. Salas, and J. M. Alameda, Phys. Rev. B **56**, 3306 (1997).
[28] S. Hameed, P. Talagala, R. Naik, L. E. Wenger, V. M. Naik, and R. Proksch, Phys. Rev. B **64**, 184406 (2001).
[29] S. Foss, C. Merton, R. Proksch, G. Skidmore, J. Schmidt, E. D. Dahlberg, T. Pokhil, and Y. T. Cheng, J. Magn. Magn. Mater. **190**, 60 (1998).
[30] R. P. Morrissey, M. Redjdal, M. F. Ruane, and F. B. Humphrey, J. Appl. Phys. **85**, 6199 (1999).
[31] S. Konings, J. Miguel, J. Goedkoop, J. Camarero, and J. Vogel, J. Appl. Phys. **100**, 033904 (2006).
[32] N. Martin, I. Mönch, R. Schäfer, J. Fassbender, L. Schultz, and J. McCord, Phys. Rev. B **83**, 174423 (2011).
[33] O. Tchernyshyov and G. W. Chern, Phys. Rev. Lett. **95**, 197204 (2005).